TESS DISCOVERY OF AN ULTRA-SHORT-PERIOD PLANET AROUND THE NEARBY M DWARF LHS 3844

Roland K. Vanderspek[1], Chelsea X. Huang[1,2], Andrew Vanderburg[3], George R. Ricker[1], David W. Latham[4], Sara Seager[1,17], Joshua N. Winn[5], Jon M. Jenkins[4], Jennifer Burt[1,2], Jason Dittmann[1,17], Elisabeth Newton[1], Samuel N. Quinn[6], Avi Shporer[1], David Charbonneau[6], Jonathan Irwin[6], Kristo Ment[6], Jennifer G. Winters[6], Karen A. Collins[6], Phil Evans[7], Tianjun Gan[8], Rhodes Hart[9], Eric L.N. Jensen[10], John Kielkopf[11], Shude Mao[8], William Waalkes[13], François Bouchy[12], Maxime Marmier[12], Louise D. Nielsen[12], Gaël Ottoni[12], Francesco Pepe[12], Damien Ségransan[12], Stéphane Udry[12], Todd Henry[20], Leonardo A. Paredes[18], Hodari-Sadiki James[18], Rodrigo H. Hinojosa[19], Michele L. Silverstein[18], Zachory Berta-Thompson[13], Misty D. Davies[4], Michael Fausnaugh[1], Ana W. Glidden[1], Joshua Pepper[14], Edward H. Morgan[1], Mark Rose[15], Joseph D. Twicken[16], Jesus Noel S. Villaseñor[1], and the TESS Team

Draft version September 17, 2018

ABSTRACT

Data from the newly-commissioned *Transiting Exoplanet Survey Satellite* (*TESS*) has revealed a "hot Earth" around LHS 3844, an M dwarf located 15 pc away. The planet has a radius of $1.404 \pm 0.035\ R_\oplus$ and orbits the star every 11 hours. Although the existence of an atmosphere around such a strongly irradiated planet is questionable, the star is bright enough ($I = 11.9$, $K = 9.1$) for this possibility to be investigated with transit and occultation spectroscopy. The star's brightness and the planet's short period will also facilitate the measurement of the planet's mass through Doppler spectroscopy.

Subject headings: planetary systems, planets and satellites: detection, stars: individual (LHS 3844)

1. INTRODUCTION

The *Transiting Exoplanet Survey Satellite* (*TESS*) is a NASA Explorer mission that was launched on April 18, 2018. The mission's primary objective is to discover hundreds of transiting planets smaller than Neptune, around stars bright enough for spectroscopic investigations of planetary masses and atmospheres (Ricker et al. 2015). Using four 10 cm refractive CCD cameras, *TESS* obtains

[1] Department of Physics and Kavli Institute for Astrophysics and Space Science, Massachusetts Institute of Technology, Cambridge, MA 02139, USA
[2] Juan Carlos Torres Fellow
[3] Department of Astronomy, The University of Texas at Austin, Austin, TX 78712, USA and NASA Sagan Fellow
[4] NASA Ames Research Center, Moffett Field, CA 94035, USA
[5] Department of Astrophysical Sciences, Princeton University, Princeton, NJ 08544, USA
[6] Harvard-Smithsonian Center for Astrophysics, 60 Garden Street, Cambridge, MA 02138, USA
[7] El Sauce Observatory, Chile
[8] Department of Physics and Tsinghua Centre for Astrophysics, Tsinghua University, Beijing, China
[9] University of Southern Queensland, Toowoomba, Queensland, Australia 4350
[10] Department of Physics and Astronomy, Swarthmore University, Swarthmore, PA 19081, USA
[11] Department of Physics and Astronomy, University of Louisville, Louisville, KY 40292, USA
[12] Observatoire de l'Université de Genève, 51 chemin des Maillettes, 1290 Versoix, Switzerland
[13] Department of Astrophysical and Planetary Sciences, University of Colorado, Boulder, CO 80309, USA
[14] Department of Physics, Lehigh University, Bethlehem, PA 18015, USA
[15] Leidos, Inc., Moffett Field, CA 94035, USA
[16] SETI Institute, Moffett Field, CA 94035, USA
[17] Department of Earth and Planetary Sciences, Massachusetts Institute of Technology, Cambridge, MA 02139, USA
[18] Department of Physics and Astronomy, Georgia State University, Atlanta, GA 30302-4106
[19] Cerro Tololo Inter-American Observatory, CTIO/AURA Inc., La Serena, Chile
[20] RECONS Institute, Chambersburg, PA, 17201

optical images of a rectangular field spanning 2300 square degrees. The field is changed every 27.4 days (two spacecraft orbits), allowing the survey to cover most of the sky in 2 years. *TESS* is a wider-field, brighter-star successor to the successful space-based transit surveys CoRoT (Barge et al. 2008; Haywood et al. 2014) and *Kepler* (Borucki et al. 2011).

Another way in which *TESS* differs from the previous space missions is that M dwarfs constitute a larger fraction of the stars being searched, mainly because of a redder observing bandpass (600–1000 nm). Compared to solar-type stars, M dwarfs are advantageous for transit surveys because the signals are larger for a given planet size, and because the transits of planets in the "habitable zone" are geometrically more likely and repeat more frequently (see, e.g., Gould et al. 2003; Charbonneau & Deming 2007; Latham 2012). We also know that close-orbiting planets are very common around M dwarfs, based on results from the *Kepler* survey (Dressing & Charbonneau 2015; Muirhead et al. 2015). By focusing on nearby M dwarfs, the pioneering ground-based transit surveys MEarth and TRAPPIST have discovered four of the most remarkable planetary systems known today: GJ 1214 (Charbonneau et al. 2009), GJ 1132 (Berta-Thompson et al. 2015), LHS 1140 (Dittmann et al. 2017b; Ment et al. 2018), and TRAPPIST-1 (Gillon et al. 2016).

Simulations have shown that *TESS* should be capable of detecting hundreds of planets around nearby M dwarfs (Sullivan et al. 2015; Bouma et al. 2017; Ballard 2018; Muirhead et al. 2018a; Barclay et al. 2018; Huang et al. 2018). Here, we report the first such detection, based on data from the first month of the survey. The planet is 1.404 ± 0.035 times larger than the Earth, and orbits the M dwarf LHS 3844 every 11 hours. The star, located 15 parsecs away, has a mass and radius that are about 15% and 19% of the Sun's values. The proximity and brightness of the star make this system a good candidate

for follow-up Doppler and atmospheric spectroscopy.

This *Letter* is organized as follows. Section 2 presents the data from *TESS* along with follow-up observations with ground-based telescopes. Section 3 describes our method for determining the system parameters. This section also explains why the transit-like signal is very likely to represent a true planet and not an eclipsing binary or other types of "false positives." Section 4 compares LHS 3844 b with the other known transiting planets, and discusses some possibilities for follow-up observations.

2. OBSERVATIONS AND DATA ANALYSIS

2.1. *TESS*

TESS observed LHS 3844 between 2018 Jul 25 and Aug 22, in the first of 26 sectors of the two-year survey. The star appeared in CCD 2 of Camera 3. The CCDs produce images every 2 seconds, which are summed onboard the spacecraft into images with an effective exposure time of 30 minutes. In addition, 2-minute images are prepared for subarrays surrounding pre-selected target stars, which are chosen primarily for the ease of detecting transiting planets. LHS 3844 was prioritized for 2-minute observations on account of its brightness in the *TESS* bandpass ($T = 11.877$), small stellar radius, and relative isolation from nearby stars (Stassun et al. 2018; Muirhead et al. 2018b).

The 2-minute data consist of 11 by 11 pixel subarrays. They were reduced with the Science Processing Operations Center (SPOC) pipeline, originally developed for the *Kepler* mission at the NASA Ames Research Center (Jenkins 2015; Jenkins et al. 2016). For LHS 3844, the signal-to-noise ratio of the transit signals was 32.4. The 30-minute data were analyzed independently with the MIT Quick Look Pipeline (QLP; Huang et al., in prep). A transit search with the Box Least Square algorithm (BLS, Kovács et al. 2002) led to a detection with a signal-to-noise ratio of 31.6.

For subsequent analysis, we used the 2-minute Presearch Data Conditioning light curve from the SPOC pipeline (Stumpe et al. 2012), which was extracted from the photometric aperture depicted in the lower right panel of Figure 1. The resulting light curve is shown in the top panel of Figure 2. To filter out low-frequency variations, we fitted a basis spline to the light curve (excluding the transits and 3σ outliers) and divided the light curve by the best-fit spline. The result is shown in the second panel of Figure 2. The interruption in the middle of the time series occurred when the spacecraft was at perigee, when it reorients and downlinks the data. There was also a 2-day interval when the data were compromised by abnormally unstable spacecraft pointing. In addition, we omitted the data collected in the vicinity of "momentum dumps," when the thrusters are used to reduce the speed of the spacecraft reaction wheels. These lasted 10–15 minutes and took place every 2.5 days.

2.2. *Ground-based Photometry*

LHS 3844 was observed by the ground-based MEarth-South telescope array as part of normal survey operations (Irwin et al. 2015; Dittmann et al. 2017a). A total of 1935 photometric observations were made between 2016 Jan 10 and 2018 Aug 25. No transits had been detected prior to the *TESS* detection, but when the data

TABLE 1
Radial Velocities of LHS 3844

BJD	RV (km s^{-1})	σ_{RV} (km s^{-1})	Instrument
2458287.9183	−10.626	0.056	CHIRON
2458287.9393	−10.667	0.108	CHIRON
2458369.6266	−10.719	0.031	CHIRON
2458369.6476	−10.732	0.046	CHIRON
2458369.6686	−10.724	0.048	CHIRON
2458371.653268	−10.600	0.090	CORALIE
2458372.780028	−10.540	0.068	CORALIE

NOTE. — The 100 m s^{-1} difference between the average CHIRON and CORALIE velocities is due to differences in the instrumental zero points, and is not indicative of velocity variation.

were revisited, a BLS search identified a signal with a period and amplitude consistent with the *TESS* signal (Figure 2). The MEarth data also reveal the stellar rotation period to be 128 days, based on the method described by Newton et al. (2016, 2018).[21]

Additional ground-based transit observations were performed as part of the *TESS* Follow-up Observing Program (TFOP). A full transit was observed on UT 2018 Sep 06 in the I_C band, using the El Sauce Observatory Planewave CDK14 telescope located in El Sauce, Chile. Five more transits were observed in the Sloan i' band using telescopes at the Cerro Tololo International Observatory (CTIO) node of the Las Cumbres Observatory.[22] The transit of UT 2018 Sep 08 was observed with a 0.4 m telescope, and the transits of UT 2018 Sep 08, 09, 10 and 16 were observed with a 1.0 m telescope. The data are shown in the lower panels of Figure 2. Together, they confirm the fading events are occurring and localize the source to within 2″ of LHS 3844.

2.3. *High-Resolution Spectroscopy*

We obtained optical spectra on UT 2018 Jun 18 and Sep 08 using the CTIO HIgh ResolutiON (CHIRON) spectrograph on the 1.5 m telescope of the CTIO Small and Moderate Aperture Research Telescope System (Tokovinin et al. 2013). We used the image slicer mode, giving a resolution of about 80,000. The first observation was a pair of 30 min exposures centered at an orbital phase of 0.355. The second observation comprised three 30 min exposures centered at phase 0.880. The data were analyzed as described by Winters et al. (2018), using a spectrum of Barnard's Star as a template. The spectra show no evidence of additional lines from a stellar companion, no sign of rotational broadening, no detectable Hα emission, and no radial velocity variation.

Additional spectroscopy was performed with the CORALIE spectrograph (Queloz et al. 2000; Pepe et al. 2017) on the Swiss Euler 1.2 m telescope at La Silla Observatory in Chile. Spectra were obtained on UT 2018 Sep 10 and 11, at phases 0.211 and 0.645, near the expected radial-velocity extrema. Radial-velocity calibration was performed with a Fabry-Pérot device. With exposure times of 45 and 60 min, the signal-to-noise

---

[21] Although Newton et al. (2018) did not detect rotational modulation, subsequent data have allowed for a "Grade B" detection, in the rating system described in that work.
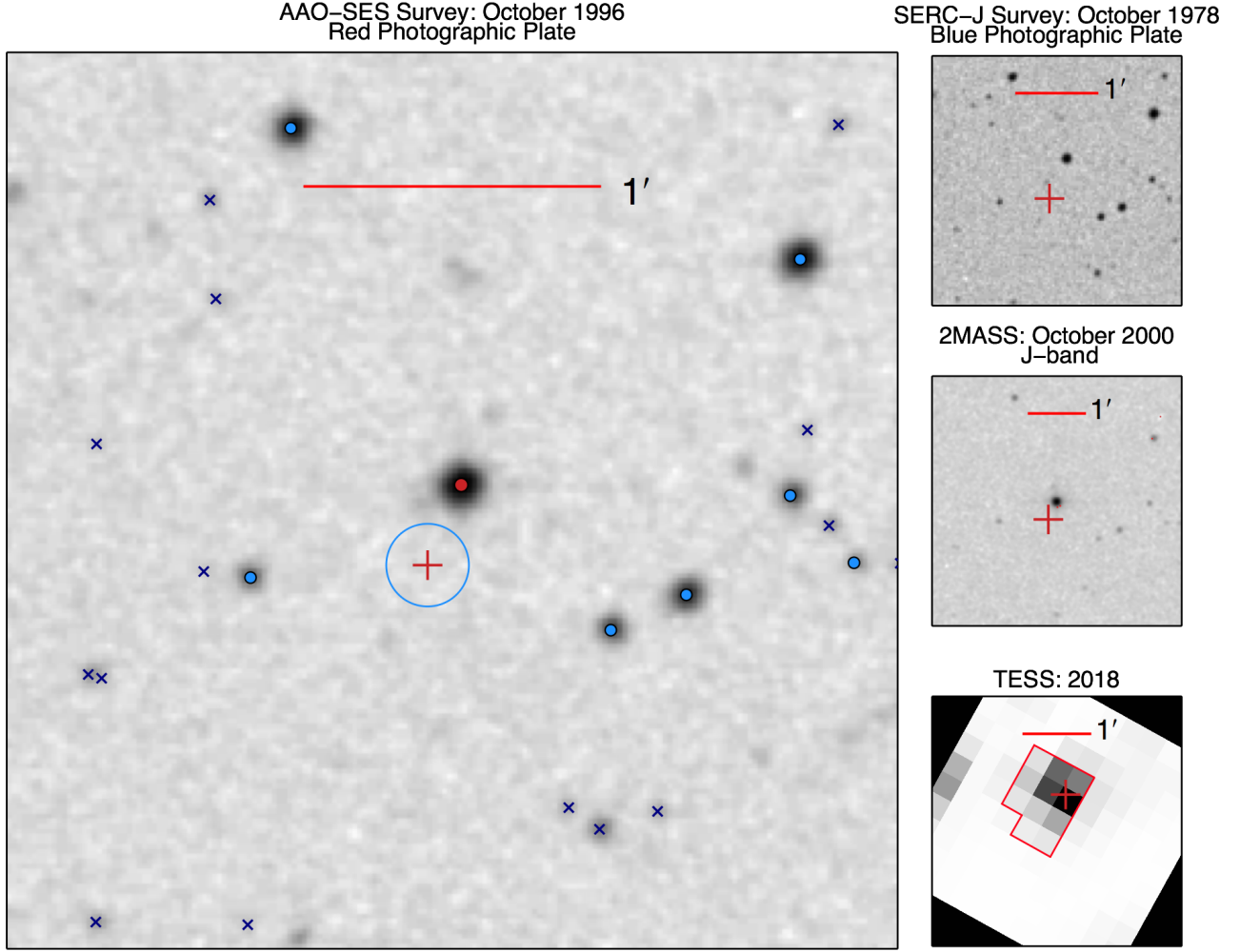
[22] https://lco.global

FIG. 1.— Images of the field surrounding LHS 3844. *Left.*—From the Anglo-Australian Observatory Second Epoch Survey, obtained with a red-sensitive photographic emulsion in 1996. The red point is the location of LHS 3844 in this image, and the red cross indicates the current position. The blue points are stars that are bright enough to potentially be the source of the transit signal, while blue crosses are stars that are too faint. The blue circle shows the 10σ upper limit on the motion of the center of light during transits. The lack of motion rules out the possibility that any of the surrounding stars is the source of the transit signal. *Upper right.*—From the Science and Engineering Research Council J survey, obtained with a blue-sensitive photographic emulsion in 1978. *Middle right.*–From the Two Micron All Sky Survey (2MASS) in *J*-band. *Lower right.*—Summed *TESS* image.

ratio per pixel was about 3 in the vicinity of 600 nm. Cross-correlations were performed with a weighted M2 binary mask from which telluric and interstellar lines were removed (Pepe et al. 2002). Only a single peak was detected. The difference in radial velocities was 60 ± 110 m s^{-1}, i.e., not statistically significant.

To place an upper limit on the radial velocity variation using both datasets (see Table 1), we fitted for the amplitude of a sinusoidal function with a period and phase specified by the *TESS* transit signal. The free parameters were the amplitude K, and two additive constants representing the zeropoints of the CHIRON and CORALIE velocity scales. The result was $K = -28^{+64}_{-60}$ m s^{-1}, which can be interpreted as a 3σ upper limit of 0.96 $M_{\rm Jup}$ on the mass of the transiting object.

3. ANALYSIS

3.1. *Stellar parameters*

Using an empirical relationship between mass and K_s-band absolute magnitude (Benedict et al. 2016), and the parallax from Data Release 2 of the *Gaia* mission (Gaia Collaboration et al. 2018; Lindegren et al. 2018), the mass of LHS 3844 is 0.151 ± 0.014 $M_\odot$. The uncertainty is dominated by the scatter in the mass-K_s relation. Based on this mass determination, and the empirical mass-radius relationship of Boyajian et al. (2012), the stellar radius is 0.188 ± 0.006 $R_\odot$. These results are consistent with the empirical relationship between radius and absolute K_s magnitude presented by Mann et al. (2015), which gives 0.189 ± 0.004 $R_\odot$. The bolometric luminosity is $(2.72 \pm 0.04) \times 10^{-3}$ $L_\odot$, based on the observed V and J magnitudes and the bolometric correction from Table 3 of Mann et al. (2015). Based on these determinations of $R_\star$ and $L_\star$, the Stefan-Boltzmann law gives an effective temperature of 3036 ± 77 K. The spectral type is M4.5 or M5, based on a comparison with MEarth survey stars of known spectral types on a color-magnitude diagram (*Gaia G* versus $H - K_s$).

3.2. *Light curve modeling*

We jointly analyzed the light curves from *TESS*, MEarth, and TFOP, using the formalism of Mandel &
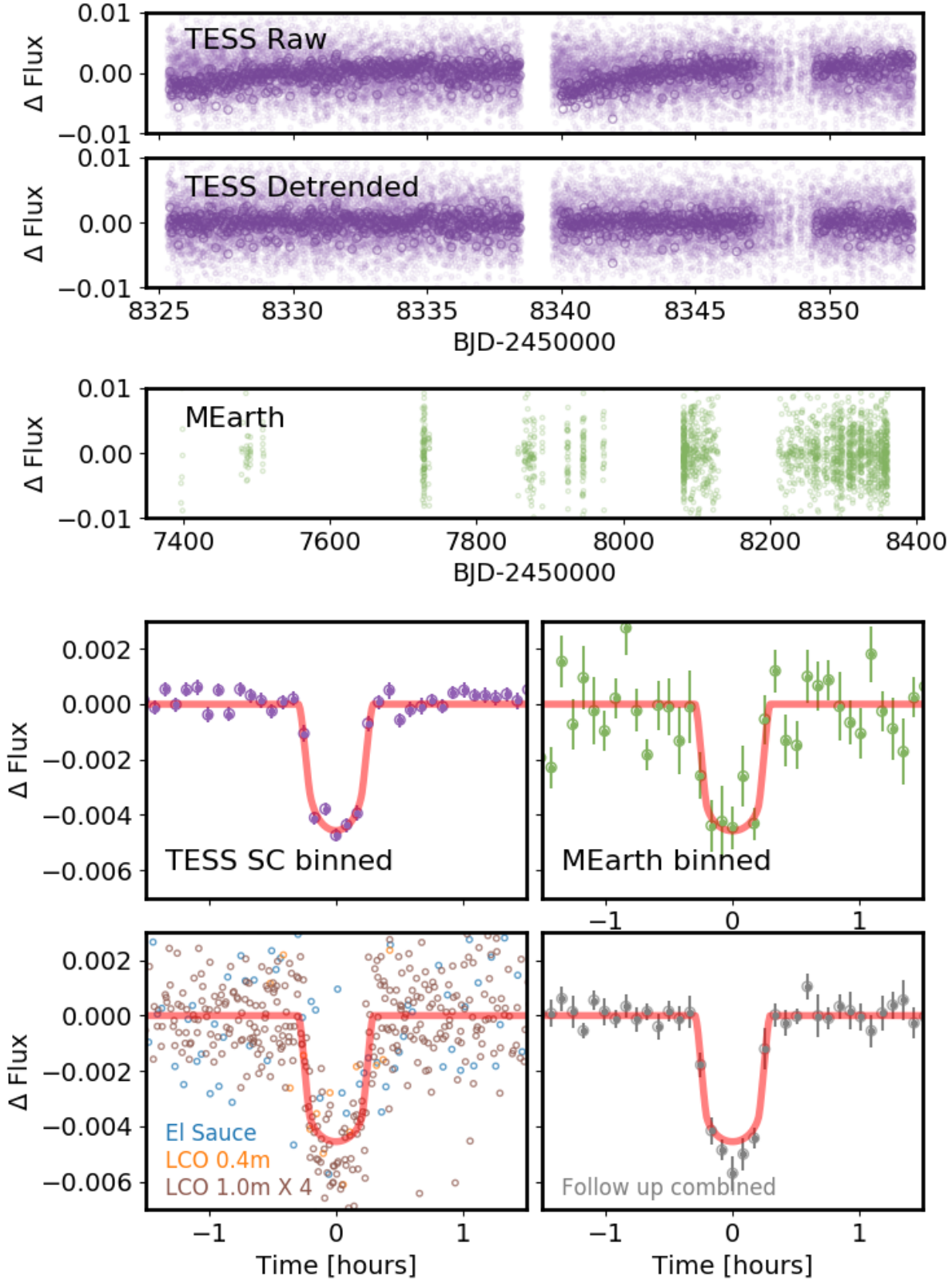
4

FIG. 2.— Light curves of LHS 3844. The top two panels show the *TESS* data, before and after high-pass filtering. The middle panel is from the MEarth Observatory, after correcting for systematics. The lower grid of four panels are phase-folded light curves, along with the best-fitting transit model. The data points with error bars represent 5 min averages. The bottom two panels show data from the *TESS* Follow-up Observing Program, both the original data and 5 min averages.
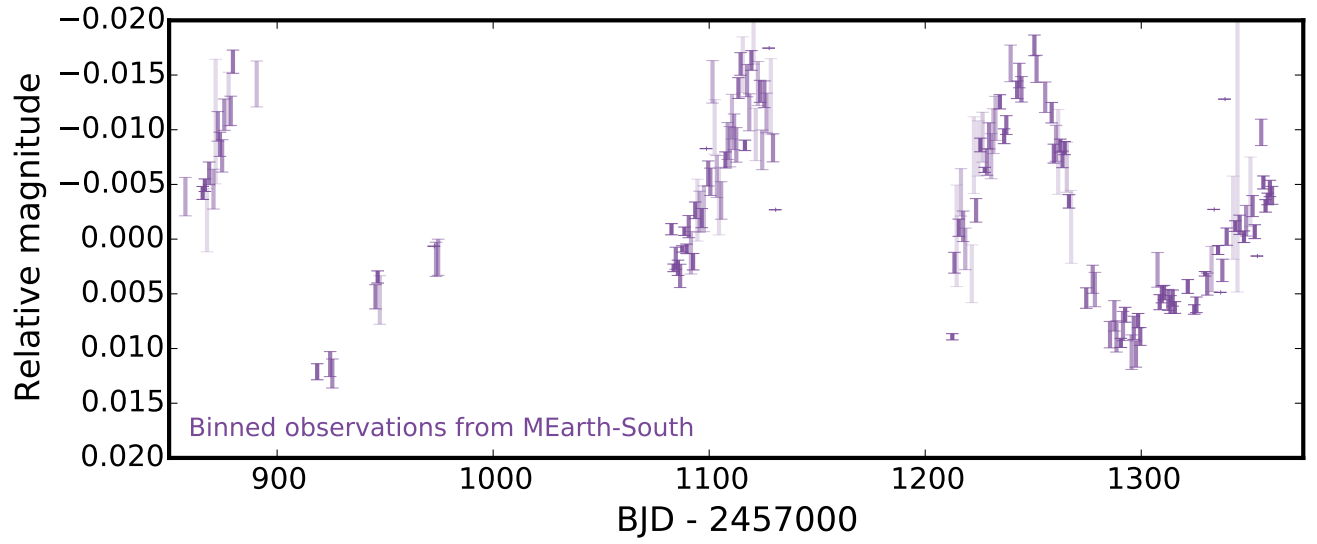
FIG. 3.— Long-term photometric monitoring of LHS 3844 by the MEarth Observatory. One-day averages are plotted, with error bars representing the standard error of the mean. Data points with higher precision are plotted with more opaque symbols. Based on the sinusoidal modulation observed in the most recent data, the rotation period is approximately 128 days.

Agol (2002) as implemented by Kreidberg (2015). We assumed the orbit to be circular, and placed Gaussian prior constraints on the two parameters of a quadratic limb-darkening law ($u_1 = 0.145 \pm 0.05$ and $u_2 = 0.54 \pm 0.05$; Claret 2017). Because of the differing bandpasses of *TESS*, MEarth, and the TFOP instruments, each dataset was allowed to have different values for the limb-darkening parameters. We imposed a prior constraint on the mean stellar density based on the results of Section 3.1. The model was evaluated with 0.4 min sampling and averaged as appropriate before comparing with the data. We used the `emcee` Monte Carlo Markov Chain code of Foreman-Mackey et al. (2013) to determine the posterior distributions for all the model parameters. The results are given in Table 2. Figure 2 shows the best-fitting model.

We also performed a fit to the *TESS* data only, without any prior constraint on the mean stellar density, in order to allow for a consistency check between the two density determinations. Based on the stellar parameters derived in Section 3.1, the mean density is 31.36 ± 0.23 g cm^{-3}, while the light-curve solution gives $30.0^{+7.4}_{-2.8}$ g cm^{-3}. The agreement between these two results is a sign that the transit signal is from a planet, and is not an astrophysical false positive. A related point is that the ratio τ/T between the ingress/egress duration and the total duration is $0.11^{+0.01}_{-0.02}$, and less than 0.14 with 99% confidence. This information is used in Section 3.2 to help rule out the possibility that the fading events are from an unresolved eclipsing binary. In general, $\tau/T \geq R_p/R_\star$, even when the photometric signal includes the constant light from an unresolved star (Morris et al. 2018).

3.3. *Photocenter motion*

Many transit-like signals turn out to be from eclipsing binaries that are nearly along the same line of sight as the intended target star, such that the light from the binary is blended together with the constant light of the intended target star. These cases can often be recognized by measuring any motion of the center of light ("centroid") associated with the fading events (Wu et al. 2010). To do so, we modeled the time series of the X and Y coordinates of the center of light as though they were light curves, after removing long-timescale trends by fitting out a cubic spline. Based on the fitted depths of the "centroid transits" we were able to put 3σ upper limits on centroid shifts of $\Delta X < 2 \times 10^{-4}$ and $\Delta Y < 6 \times 10^{-4}$ pixels, corresponding to 4.4 and 13.2 mas. Thus, there is no evidence for photocenter motion.

3.4. *Possible False Positives*

As mentioned previously, not all transit-like signals are from transiting planets. Below, we consider the usual alternatives to a transiting planet, and explain how the available data render them very unlikely.

1. *The signal is an instrumental artifact.* This is ruled out by the detection of the transit signals with ground-based telescopes (Section 2).

2. *LHS 3844 is an eclipsing binary star.* This is ruled out by the upper limit on radial-velocity variations, corresponding to a secondary mass of 0.96 $M_{\rm Jup}$ (Section 2.3). In addition, the absence of detectable phase variations in the *TESS* light curve requires that any companion be sub-stellar. An $80 M_{\rm Jup}$ companion would have produced ellipsoidal variations of order 0.1% (see, e.g., Shporer 2017), which can be excluded.

3. *Light from a distant eclipsing binary, or a distant star with a transiting planet, is blended with that of LHS 3844.* We can rule out this possibility thanks to the star's high proper motion (800 mas yr^{-1}). Because the star moves quickly relative to background stars, images from previous wide-field surveys allow us to check for faint stars along the current line of sight. No sources are detected within 6 mag of LHS 3844, the brightness level that would be required to produce 0.4% flux dips. In addition, the ground-based observations require the fading source to be within $2''$ of LHS 3844 (Section 2.2), and the *TESS* images reveal no detectable motion of the stellar image during transits (Section 3.3).

4. *LHS 3844 is physically associated with an eclipsing binary star.* The light-curve analysis (Section 3.2) requires the eclipsing object to be smaller than 14% of the size of the eclipsed star. Since the spectrum is that of an M4-5 dwarf, any secondary star would need to be of that size or smaller, implying that the eclipsing object is smaller than $0.14 \times 0.15 R_\odot$ or 2.3 $R_\oplus$. This rules out a stellar binary.

5. *LHS 3844 is a binary star and the transiting planet is around the secondary star.* The companion would have to be faint and close to LHS 3844 in order to escape detection by *Gaia* (Ziegler et al. 2018; Rizzuto et al. 2018). Another indication that any secondary star needs to be faint is that the *Gaia* parallax and apparent magnitude are consistent with the properties of a single M dwarf. However, if the transiting planet is around such a faint companion, then the true transit depth must be less than about 2% in order for the transiting object to be smaller than about 14% the size of the eclipsed star. Thus, in order to produce the 0.4% transit we observe, a secondary star would have to contribute at least 20% of the total flux in the TESS aperture while still escaping detection by *Gaia* and seeing-limited imaging.

Thus, almost all of these scenarios are ruled out, except for the possibility that the planet is actually orbiting a low-luminosity secondary star. This scenario seems contrived, and is *a priori* unlikely because of the low companion fraction for mid M dwarfs (Winters et al. 2018), the small parameter space for companions which could produce the transits we observe, the lower probability for an M dwarf to host a larger planet compared to a 1.4 $R_\oplus$ planet (Berta et al. 2013; Mulders et al. 2015), and the tendency of selection effects to favor finding transits around primary stars (Bouma et al. 2018). Probably the only way to rule out this possibility, or more exotic scenarios, is through precise Doppler monitoring.

4. DISCUSSION

LHS 3844 b is one of the closest known planets, both in terms of its distance from the Earth, and its distance
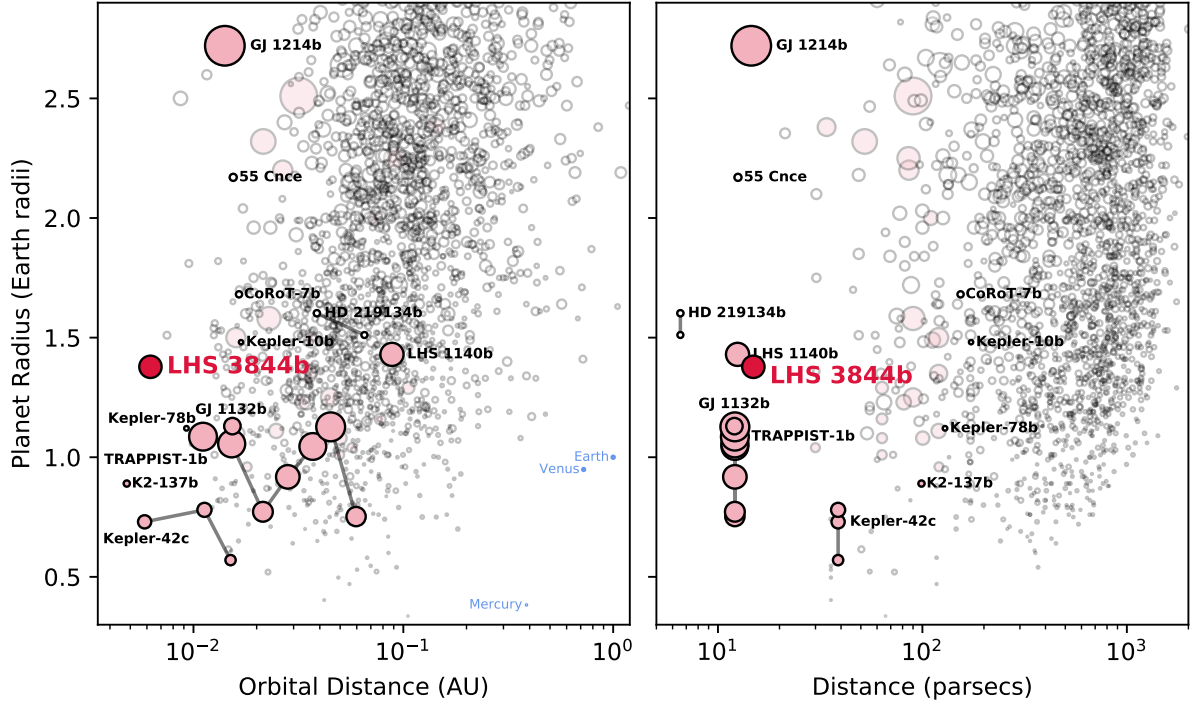
Fig. 4.— LHS 3844 b in the context of other known exoplanets. *Left.*—Planet radius and orbital distance for confirmed transiting planets. *Right.*—Planet radius and distance from Earth. The area of each circle is proportional to the transit depth of the planet. Pink circles represent host stars with $T_{\rm eff} < 3500$ K. Planets in the same system are connected by lines. Based on data from the NASA Exoplanet Archive, accessed on 13 September 2018[a].

[a]https://exoplanetarchive.ipac.caltech.edu/cgi-bin/TblView/nph-tblView?app=ExoTbls&config=planets

from its host star (see Figure 4). It joins the small club of transiting planets around the Sun's nearest M dwarf neighbors, which also includes GJ 1214 b (Charbonneau et al. 2009), GJ 1132 b (Berta-Thompson et al. 2015), TRAPPIST-1 b-h (Gillon et al. 2016), and LHS 1140 b-c (Dittmann et al. 2017b; Ment et al. 2018). LHS 3844 b is also the most easily studied example of an ultra-short-period (USP) planet, defined by the simple criterion $P < 1$ day (Sanchis-Ojeda et al. 2014; Winn et al. 2018). It has the largest transit depth of any known sub-Jovian USP planet, and is brighter and closer to Earth than the other well-known systems CoRoT-7 (Léger et al. 2009), Kepler-10 (Batalha et al. 2011), Kepler-42 (Muirhead et al. 2012), and Kepler-78 (Sanchis-Ojeda et al. 2013).

As such, LHS 3844 b provides interesting opportunities for atmospheric characterization through transit and occultation (secondary eclipse) spectroscopy. With an equilibrium temperature of about 1000 K, and an orbital distance amounting to only 4.4 stellar radii, it is unclear what type of atmosphere the planet might have, if any. If the planet formed at or near this location, its primordial atmosphere could have been completely stripped away during the host star's youth, when it was much more luminous and chromospherically active. The observed radius function of the short-period *Kepler* planets has a dip at around 1.8 $R_\oplus$ that has been interpreted as a consequence of atmospheric loss. Planets smaller than 1.8 $R_\oplus$

seem to have lost their primordial hydrogen-helium atmospheres due to photoevaporation (Fulton et al. 2017; Lopez & Fortney 2013; Owen & Wu 2013). With a radius of 1.4 $R_\oplus$, we might expect LHS 3844 b to have suffered this process, too. In this case, transit spectroscopy would show no variation in the planetary radius with wavelength, although occultation spectroscopy could still be used to measure the emission spectrum of the planet's surface.

Indeed, of all the known planets smaller than 2 $R_\oplus$, LHS 3844 b has the most readily detectable occultations. This is based on a ranking of the 907 planets in the NASA Exoplanet Archive by a crude signal-to-noise metric,

$$\mathrm{S/N} \propto \sqrt{F_\star}\ \frac{R_p^2 T_p}{R_\star^2 T_\star}, \qquad (1)$$

which assumes that the star and planet are both radiating as blackbodies in the Rayleigh-Jeans limit. Here, $F_\star$ is the star's K-band flux, T_p is the planet's equilibrium temperature, and $T_\star$ is the star's effective temperature. LHS 3844 b scores the highest according to this metric, and the planet's ultra-short-period will make it easier to schedule observations.

The ultra-short period will also facilitate the measurement of the planet's mass through Doppler spectroscopy. Short periods lead to stronger signals: assuming the

planet's mass is 3.5 $M_\oplus$, as it would be for a terrestrial composition, the expected semiamplitude of the Doppler signal is 10 m s^{-1}, which is unusually high for a rocky planet. The orbital period is short enough for the signal to be measured in its entirety in just a few nights. The orbital period is also 280 times shorter than the stellar rotation period, allowing for a clear separation of timescales between the orbital motion and any spurious Doppler signals related to stellar activity.

The discovery of a terrestrial planet around a nearby M dwarf during the first *TESS* observing sector suggests that the prospects for future discoveries are bright. It is worth remembering that 90% of the sky has not yet been surveyed by either *TESS* or *Kepler*.

REFERENCES

Ballard, S. 2018, ArXiv e-prints, arXiv:1801.04949

Barclay, T., Pepper, J., & Quintana, E. V. 2018, ArXiv e-prints, arXiv:1804.05050

Barge, P., Baglin, A., Auvergne, M., et al. 2008, A&A, 482, L17

Batalha, N. M., Borucki, W. J., Bryson, S. T., et al. 2011, ApJ, 729, 27

Benedict, G. F., Henry, T. J., Franz, O. G., et al. 2016, AJ, 152, 141

Berta, Z. K., Irwin, J., & Charbonneau, D. 2013, ApJ, 775, 91

Berta-Thompson, Z. K., Irwin, J., Charbonneau, D., et al. 2015, Nature, 527, 204

Borucki, W. J., Koch, D. G., Basri, G., et al. 2011, ApJ, 736, 19

Bouma, L. G., Masuda, K., & Winn, J. N. 2018, AJ, 155, 244

Bouma, L. G., Winn, J. N., Kosiarek, J., & McCullough, P. R. 2017, ArXiv e-prints, arXiv:1705.08891

Boyajian, T. S., von Braun, K., van Belle, G., et al. 2012, ApJ, 757, 112

Charbonneau, D., & Deming, D. 2007, ArXiv e-prints, arXiv:0706.1047

Charbonneau, D., Berta, Z. K., Irwin, J., et al. 2009, Nature, 462, 891

Claret, A. 2017, A&A, 600, A30

Dittmann, J. A., Irwin, J. M., Charbonneau, D., Berta-Thompson, Z. K., & Newton, E. R. 2017a, AJ, 154, 142

Dittmann, J. A., Irwin, J. M., Charbonneau, D., et al. 2017b, Nature, 544, 333

Dressing, C. D., & Charbonneau, D. 2015, ApJ, 807, 45

Foreman-Mackey, D., Hogg, D. W., Lang, D., & Goodman, J. 2013, PASP, 125, 306

Fulton, B. J., Petigura, E. A., Howard, A. W., et al. 2017, AJ, 154, 109

Gaia Collaboration, Brown, A. G. A., Vallenari, A., et al. 2018, A&A, 616, A1

Gillon, M., Jehin, E., Lederer, S. M., et al. 2016, Nature, 533, 221

Gould, A., Pepper, J., & DePoy, D. L. 2003, ApJ, 594, 533

Haywood, R. D., Collier Cameron, A., Queloz, D., et al. 2014, MNRAS, 443, 2517

Huang, C. X., Shporer, A., Dragomir, D., et al. 2018, ArXiv e-prints, arXiv:1807.11129

Irwin, J. M., Berta-Thompson, Z. K., Charbonneau, D., et al. 2015, in 18th Cambridge Workshop on Cool Stars, Stellar Systems, and the Sun, Vol. 18, 767–772

Jao, W.-C., Henry, T. J., Subasavage, J. P., et al. 2005, AJ, 129, 1954

Jenkins, J. M. 2015, in AAS/Division for Extreme Solar Systems Abstracts, Vol. 3, AAS/Division for Extreme Solar Systems Abstracts, 106.05

Jenkins, J. M., Twicken, J. D., McCauliff, S., et al. 2016, in Proc. SPIE, Vol. 9913, Software and Cyberinfrastructure for Astronomy IV, 99133E

Kovács, G., Zucker, S., & Mazeh, T. 2002, A&A, 391, 369

Kreidberg, L. 2015, PASP, 127, 1161

Latham, D. W. 2012, Nature, 56, 16

Léger, A., Rouan, D., Schneider, J., et al. 2009, A&A, 506, 287

Lindegren, L., Hernández, J., Bombrun, A., et al. 2018, A&A, 616, A2

Lopez, E. D., & Fortney, J. J. 2013, ApJ, 776, 2

Mandel, K., & Agol, E. 2002, ApJ, 580, L171

Mann, A. W., Feiden, G. A., Gaidos, E., Boyajian, T., & von Braun, K. 2015, ApJ, 804, 64

Ment, K., Dittmann, J. A., Astudillo-Defru, N., et al. 2018, ArXiv e-prints, arXiv:1808.00485

Morris, B. M., Agol, E., Hebb, L., & Hawley, S. L. 2018, AJ, 156, 91

Muirhead, P. S., Dressing, C. D., Mann, A. W., et al. 2018a, AJ, 155, 180

—. 2018b, AJ, 155, 180

Muirhead, P. S., Johnson, J. A., Apps, K., et al. 2012, ApJ, 747, 144

Muirhead, P. S., Mann, A. W., Vanderburg, A., et al. 2015, ApJ, 801, 18

Mulders, G. D., Pascucci, I., & Apai, D. 2015, ApJ, 814, 130

Newton, E. R., Irwin, J., Charbonneau, D., Berta-Thompson, Z. K., & Dittmann, J. A. 2016, ApJ, 821, L19

Newton, E. R., Mondrik, N., Irwin, J., Winters, J. G., & Charbonneau, D. 2018, ArXiv e-prints, arXiv:1807.09365

Owen, J. E., & Wu, Y. 2013, ApJ, 775, 105

Pepe, F., Bouchy, F., Mayor, M., & Udry, S. 2017, High-Precision Spectrographs for Exoplanet Research: CORAVEL, ELODIE, CORALIE, SOPHIE and HARPS, 190

Pepe, F., Mayor, M., Galland, F., et al. 2002, A&A, 388, 632

Queloz, D., Mayor, M., Weber, L., et al. 2000, A&A, 354, 99

Ricker, G. R., Winn, J. N., Vanderspek, R., et al. 2015, Journal of Astronomical Telescopes, Instruments, and Systems, 1, 014003

Rizzuto, A. C., Vanderburg, A., Mann, A. W., et al. 2018, ArXiv e-prints, arXiv:1808.07068

Sanchis-Ojeda, R., Rappaport, S., Winn, J. N., et al. 2014, ApJ, 787, 47

—. 2013, ApJ, 774, 54

Shporer, A. 2017, PASP, 129, 072001

Stassun, K. G., Oelkers, R. J., Pepper, J., et al. 2018, AJ, 156, 102

Stumpe, M. C., Smith, J. C., Van Cleve, J. E., et al. 2012, PASP, 124, 985

Sullivan, P. W., Winn, J. N., Berta-Thompson, Z. K., et al. 2015, ApJ, 809, 77

Tokovinin, A., Fischer, D. A., Bonati, M., et al. 2013, PASP, 125, 1336

Winn, J. N., Sanchis-Ojeda, R., & Rappaport, S. 2018, ArXiv e-prints, arXiv:1803.03303

Winters, J. G., Henry, T. J., Lurie, J. C., et al. 2015, AJ, 149, 5

Winters, J. G., Irwin, J., Newton, E. R., et al. 2018, AJ, 155, 125

Wu, H., Twicken, J. D., Tenenbaum, P., et al. 2010, in Proc. SPIE, Vol. 7740, Software and Cyberinfrastructure for Astronomy, 774019

Ziegler, C., Law, N. M., Baranec, C., et al. 2018, ArXiv e-prints, arXiv:1806.10142

TABLE 2
Stellar and Planet Parameters for LHS 3844

Parameter	Value	Source
Catalog Information		
R.A. (h:m:s)	22:41:59.089	Gaia DR2
Dec. (d:m:s)	-69:10:19.59	Gaia DR2
Epoch	2015.5	Gaia DR2
Parallax (mas)	67.155 ± 0.051	Gaia DR2
μ_{ra} (mas yr^{-1})	334.357 ± 0.083	Gaia DR2
μ_{dec} (mas yr^{-1})	-726.974 ± 0.086	Gaia DR2
Gaia DR2 ID	6385548541499112448	
TIC ID	410153553	
LHS ID	3844	
TOI ID	136	
Photometric properties		
$TESS$ (mag)	11.877	TIC V7
$Gaia$ (mag)	13.393	Gaia DR2
Gaia RP (mag)............	12.052	Gaia DR2
Gaia BP (mag)............	15.451	Gaia DR2
V_J (mag)...................	15.26 ± 0.03	RECONS[a]
R_{KC} (mag)	13.74 ± 0.02	RECONS[a]
I_{KC} (mag)	11.88 ± 0.02	RECONS[a]
J (mag)...................	10.046 ± 0.023	2MASS
H (mag)	9.477 ± 0.023	2MASS
K_s (mag)	9.145 ± 0.023	2MASS
Derived properties		
$M_\star$ ($M_\odot$)	0.151 ± 0.014	Parallax +Benedict et al. (2016)[b]
$R_\star$ ($R_\odot$)	0.189 ± 0.006	Parallax +Mann et al. (2015) [c]
$\log g_\star$ (cgs)................	5.06 ± 0.01	empirical relation + LC [d]
$L_\star$ ($L_\odot$)....................	0.00272 ± 0.0004	Mann et al. (2015)
$T_{\mathrm{eff}\star}$ (K)	3036 ± 77	[e]
M_V (mag).................	14.39 ± 0.02	Parallax
M_K (mag)	8.272 ± 0.015	Parallax
Distance (pc)..............	14.9 ± 0.01	Parallax
$\rho_\star$ (g cm^{-3})................	31.38 ± 0.22	empirical relation + LC [d]
Light curve parameters		
P (days)	0.46292927 ± 0.0000031	
T_c (BJD $-$ 2457000) [b]	1325.72581 ± 0.00025	
T_{14} (min) [b]	34.74 ± 0.93	
$T_{12} = T_{34}$ (min) [b]	$3.73^{+0.4}_{-0.7}$	
$a/R_\star$	$4.39^{+0.027}_{-0.045}$	
$R_p/R_\star$	0.0679 ± 0.002	
$b \equiv a \cos i/R_\star$	0.789 ± 0.0015	
i (deg)	79.62 ± 0.17	
Limb-darkening coefficients		
c_1, MEarth (linear term) ...	0.05 ± 0.05	
c_2, MEarth (quadratic term)	0.50 ± 0.05	
$c_1, TESS$	0.28 ± 0.08	
$c_2, TESS$	0.54 ± 0.06	
c_1, i	0.21 ± 0.05	
c_2, i	0.37 ± 0.08	
Planetary parameters		
R_p ($R_\oplus$)	1.404 ± 0.035	
a (AU)	0.003872 ± 0.00016	
T_{eq} (K)	1025 ± 26	
$\langle F_j \rangle$ (10^9 erg s^{-1} cm^{-2})	0.250 ± 0.025	

[a] The optical photometry is from the RECONS survey, and was measured according to the procedures described in Jao et al. (2005); Winters et al. (2015).

[b] We adopted the error bar based on the scatter in the empirical relations described by Benedict et al. (2016).

[c] We adopted the error bar based on the scatter in the empirical relations described by Mann et al. (2015).

[d] We fitted the transit light curves with a prior constraint on the stellar density.

[e] The effective temperature was determined from the bolometric luminosity and the stellar radius.